same 5.5 × 12 cm column of SiO_2 eluted with eluant C. The proper fractions were combined and evaporated to a pale white solid by rotary evaporation using alternating azeotropes of 3 × 200 mL of toluene and 3 × 200 mL of *n*-heptane. Drying the isolated solid product overnight in vacuo (0.01 mmHg) followed by lyophilization from 25 mL of water gave 0.340 g (25%) of a light, pale-yellow solid: mp 205 °C slow dec; TLC (SiO_2) R_f 0.82 and 0.26 (eluants A and C), positive by ninhydrin, *p*-anisaldehyde, UV; $[\alpha]^{22.5}_D$ +16.5°; ^{1}H NMR (300 MHz, DMSO-d_6) δ 7.48 (d, J = 7.26 Hz, 2 H), 7.11 (d, J = 7.38 Hz, 2 H), 5.77 (br s, 14 H), 4.66 (shoulder, 1 H), 4.61 (br s, 6 H, H1), 4.53 (br s, 6 H), 3.75–3.43 (m, 28 H), 3.43–3.20 (m, overlaps with HOD), 3.13 (br t, 2 H), 2.77–2.51 (m, 2 H), 2.27 (s, 3 H), 1.62–1.37 (m, 2 H), 1.22 (s, 24 H), 0.84 (br t, J = 6.90 Hz, 3 H) ppm; ^{1}H NMR (300 MHz, D_2O) δ 7.53 (d, J = 7.73 Hz, 2 H), 7.21 (d, J = 7.86 Hz, 2 H), 5.03–4.90 (m, 7 H), 3.88–3.63 (m, 21 H), 3.63–3.20 (m, 21 H), 3.04 (br t, 2 H), 2.89–2.73 (m, 2 H), 2.26 (s, 3 H), 1.61–1.53 (m, 2 H), 1.22 (s, 14 H), 1.15 (br s, 10 H), 0.85 (t, J = 6.78 Hz) ppm; ^{13}C NMR (75 MHz, DMSO-d_6) δ 145.4 (s), 133.1 (s), 127.9 (d), 125.4 (d), 101.9 (d), 83.5 (d), 81.6 (d), 74.6–71.1 (m), 70.5 (d), 59.9 (t), 49.4 (t), 31.2 (t), 29.5, 28.9, 28.6, 26.7, 22.0, 14.0 (br s) ppm; IR (KBr) ν = 1320 (O=S=O) cm^{-1}.

Mono-6-deoxy-6-(hexadecylamino)-β-cyclodextrin Hydrochloride (5). A Sephadex CM-25 ion-exchange column was prepared by suspending 10 g (dry weight) of the stationary phase in 300 mL 3:2 ethylene glycol/water (degassed in suction flask under aspirator vacuum for 300 min) for 2 h. The suspension was degassed in a similar manner (45 min) prior to forming a bed of 3 × 11.5 cm. After equilibration, β-CDNH$_2$C$_{16}^+$-OTs$^-$ (0.125 g) was dissolved in 5 mL of eluant and adsorbed onto the column and eluted with a gradient of 3:2 ethylene glycol/water to 3:2 ethylene glycol/0.25 M aqueous NaCl (or NH_4Cl). Fractions (12 mL each) were analyzed either by optical rotation or TLC. The appropriate fractions were combined and concentrated by rotary evaporation to a light yellow solution (ca. 60 mL). Dilution to 750 mL with acetone produced a cloudy suspension and suction filtration led to recovery of a white solid which was triturated rapidly with 25 mL followed by 5 mL followed by another 5 mL of cold water. The remaining residue was dried overnight in vacuo (0.01 mmHg), and the three supernatants were lyophilized. The remaining residue was revealed to be pure product (white solid; 0.108 g, 95%): mp 222 °C slow dec; TLC (SiO_2) R_f 0.77, 0.69, 0.24 (eluants A, B, C), ninhydrin and *p*-anisaldehyde positive, R_f 0.14 (reversed phase, eluant D), *p*-anisaldehyde positive; $[\alpha]^{21.5}_D$ +18.3°; ^{1}H NMR (300 MHz, DMSO-d_6) δ 5.80–5.61 (m, 14 H), 4.93 (br s, 1 H), 4.82 (br s, 6 H), 4.62–4.52 (m, 6 H), 3.85–3.45 (m, 28 H), 3.45–3.20 (m, overlaps with HOD), 3.10 (br t, 2 H), 2.85–2.72 (m, 2 H), 1.62–1.45 (m, 2 H), 1.22 (s, 24 H), 0.84 (t, J = 6.89 Hz, 3 H) ppm; ^{1}H NMR (300 MHz, D_2O) δ 5.04–4.97 (m, 3 H), 4.95 (br s, 4 H), 3.84–3.65 (m, 21 H), 3.63–3.41 (m, 21 H), 3.26 (br t, 2 H), 2.90–2.77 (m, 2 H), 1.61–1.51 (m, 2 H), 1.26 (s, 14 H), 1.19 (br s, 10 H), 0.82 (t, 3 H, J = 6.80 Hz) ppm; ^{13}C NMR (75 MHz, DMSO-d_6) 102.1 (d), 101.6 (s), 83.6 (d), 82.3 (s), 81.7 (d), 73.3–71.8 (m), 62.9 (d), 60.6 (s), 60.1 (t), 48.2 (t), 31.5 (t), 29.2, 26.3, 22.3 (br s), 14.2 (q) ppm; IR (KBr) ν = 2865 cm^{-1}; FAB-MS, m/z calcd for $C_{58}H_{104}NO_{34}$ (M^+ - Cl) 1358.64, measured 1358.54. Anal. Calcd for $C_{58}H_{104}ClNO_{34}\cdot 8H_2O\cdot 2NaCl$: C, 42.07; N, 0.85; Cl, 6.42. Found: C, 42.31; N, 0.90; Cl, 6.24.

Mono-6-deoxy-6-(didecylamino)-β-cyclodextrin Acetate (6). Didecylamine (462 mg, 1.55 mmol) was dissolved in dry DMF (4.0 mL) and the flask warmed to 75 °C. DMAP (194 mg, 1.59 mmol), KI (64.4 mg, 0.388 mmol), and β-CDOTs (1.00 g, 0.776 mmol) were added to the reaction mixture to give a clear yellow solution. After 24 h at 75 °C the reaction was cooled to 23 °C, and the volatile materials were removed in vacuo (0.01 mmHg, 8 H). The resulting yellow viscous oil was treated with 25 mL of cold water and the ensuing white precipitate collected by filtration. Allowing the clear filtrate to stand at 23 °C for 24 h afforded a second crop of precipitate. The combined crops were purified by flash chromatography (SiO_2, 5.5 × 13.5 cm, eluant C). A pale-white solid was obtained (277 mg, 24%): mp 212 °C dec; TLC (SiO_2) R_f 0.86, 0.70, 0.23 (eluants A, B, C) positive by *p*-anisaldehyde; TLC (reversed phase) R_f 0.24 (eluant D) *p*-anisaldehyde positive; $[\alpha]^{23.0}_D$ +13.3°; ^{1}H NMR (300 MHz, DMSO-d_6) δ 4.85–4.71 (br m, 7 H,), 3.80–3.45 (m, 28 H), 3.45–3.15 (br s, overlaps with HOD), 1.81–1.65 (br s), 1.53–1.39 (br m, 4 H), 1.23 (br s, 20 H), 1.19 (br s, 12 H), 0.86 (t, J = 6.77 Hz, 6 H) ppm; ^{1}H NMR (300 MHz, D_2O) δ 5.12–5.01 (br m, 7 H), 3.95–3.68 (m, 21 H), 3.68–3.42 (m, 21 H), 3.05 (br t, 4 H), 1.81–1.66 (br s), 1.52–1.32 (br m, 4 H), 1.23 (s, 24 H), 1.19 (br s, 8 H), 0.86 (t, J = 6.60 Hz) ppm; ^{13}C NMR (75 MHz, DMSO-d_6): δ 165.71, 102.39, 100.72, 84.00, 81.59, 74.50–71.11, 67.43, 61.19, 60.72, 50.40, 34.78, 28.01, 27.55, 23.39, 15.61 ppm; IR (KBr) ν = 2875 cm^{-1}; FAB-MS, m/z calcd for $C_{62}H_{112}NO_{34}$ (M - OAc) 1446.70, measured 1446.43.

Acknowledgment. This work was supported by grants from the NIH (Grant No. GM37235) and the Univeristy of Pittsburgh Office of Research. We thank Drs. James Brady and William Gordon for advice and technical assistance and Prof. David Waldeck for many stimulating conversations.

Supplementary Material Available: Six figures including a graph of conductivity vs time and ^{1}H NMR spectra of **5**, graph of binding isotherms for β-CD and CCA titrated against 4-NP and **3**, respectively, and NOESY and COSY spectra of **4** (6 pages). Ordering information is given on any current masthead page.

Symmetric Intramolecular Proton Transfers between Oxygen Atoms in Anionic Systems. An ab Initio Study

Enric Bosch, José M. Lluch,* and Juan Bertrán

Contribution from the Departament de Química, Universitat Autònoma de Barcelona, 08193 Bellaterra, Spain. *Received May 22, 1989*

Abstract: Three symmetric intramolecular proton exchanges involving oxygen atoms in negatively charged systems have been studied by ab initio methods. An important rearrangement of the electronic charge density takes place as the reactions proceed. The O–O bond is broken in the hydroperoxide anion at the transition state, the energy barrier being very large. In the water–hydroperoxide anion complex the water molecule acts as a bifunctional catalyst, the O–O bond remaining formed and the energy barrier being significantly lowered. Finally, the proton transfer in the glycolate anion occurs through a C_{2v} transition state whose total electronic charge density presents a ring point, the energy barrier being very small.

I. Introduction

Proton transfer reactions are one of the most important problems in chemical and biochemical systems.[1,2] Understanding and modeling of all factors involved in such transfers is a very interesting challenge for theoretical chemistry. An accurate description of the most relevant regions of the potential energy hypersurfaces is required as a first step, in this way supplying information that is not easily available from experiment and providing a starting point for a later modeling on the dynamics of the proton transfer. In recent years ab initio molecular orbital methods have become an important tool in the study of this field.

(1) Caldin, E. F., Gold, V., Eds. *Proton-Transfer Reactions*; Chapman and Hall: London, 1975.
(2) Page, M. T. *The Chemistry of Enzyme Action*; Elsevier: Amsterdam, 1974.

0002-7863/90/1512-3868$02.50/0

Since most proton transfers in biological systems involve oxygen and/or nitrogen atoms, a lot of earlier theoretical works[3-16] have dealt with proton transfers between oxygen atoms in a wide variety of molecules. However, to our knowledge, an intramolecular proton transfer between two equivalent oxygen atoms, the proton-acceptor oxygen atom being negatively charged, has not been theoretically studied yet. This is an interesting process that could play an important role in some biochemical systems. For example, the relatively high acidity of sugar hydroxyls in ribonucleosides has been ascribed[17-19] to the cis 2′-OH and 3′-OH and the ability of these to hydrogen bond in the anion. For that reason we will focus in this paper on the symmetric intramolecular proton exchange between oxygen atoms in negatively charged systems.

To this purpose, we have first studied the simplest reaction of this type: the intramolecular proton transfer in the hydroperoxide anion (HO_2^-), which is known to be a Brønsted base in the gas phase.[20,21] Moreover, in order to elucidate if a double proton transfer is a favorable process in the present case, we have also investigated the effect of adding one water molecule to the hydroperoxide anion. As a matter of fact, several proton transfer reactions in which water molecules, acting as solvent, are actively involved along the reaction pathway, and therefore leading to a change of the molecular mechanism, have been previously reported.[22-38]

The systems proposed above are very simple models. Finally we have studied a more realistic reaction, the intramolecular proton exchange in the glycolate anion. From the analysis of the results obtained in this work we expect to be able to discuss which are the factors that control the main features of the potential energy hypersurfaces of this kind of proton transfer reaction. An elucidation of the mechanism of the prototype reactions studied here can represent the first step in order to achieve a good understanding of the behavior of more complex systems.

In section II of this paper we describe the theoretical method. Intramolecular proton transfer in the hydroperoxide anion is studied in section III. Intramolecular proton transfer in the water-hydroperoxide anion complex is discussed in section IV. Results corresponding to the glycolate anion are given in section V. Finally, in section VI the main conclusions of this work are given.

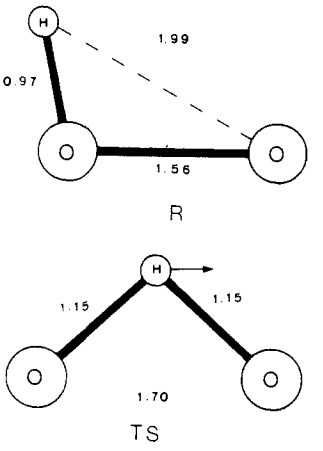

Figure 1. Geometries of the reactant (R) and transition state (TS) for the intramolecular proton transfer in HO_2^-. The arrow in the TS structure indicates the transition vector.

Table I. Potential Energy[a] Barriers for the Intramolecular Proton Transfer in the Hydroperoxide Anion

$\Delta E^{\ddagger}$ (3-21+G//3-21+G)	32.6
$\Delta E^{\ddagger}$ (6-31+G//3-21+G)	35.6
$\Delta E^{\ddagger}$ (6-31+G(D,P)//3-21+G)	32.6
$\Delta E^{\ddagger}$ (MP2/6-31+G//3-21+G)	17.5
$\Delta E^{\ddagger}$ (MP2/6-31+G(D,P)//3-21+G)	15.6
$\Delta E^{\ddagger}$ (MP3/6-31+G//3-21+G)	26.0
$\Delta E^{\ddagger}$ (MP3/6-31+G(D,P)//3-21+G)	23.1

[a] In kcal/mol.

II. Theoretical Method

Ab initio self-consistent field (SCF) calculations have been carried out with the GAUSSIAN 86 series of programs,[39] using the triply split valence basis set 3-21+G,[40,41] which contains a diffuse sp shell on atoms other than hydrogen. Diffuse functions are well-known to be important for describing the electronic structure of anions, particularly with first-row elements.

Given that every transfer treated in this paper is intramolecular, structural constraints imposed by the entire system determine the orientation and the distance between the proton donor and the proton acceptor groups, artificial restraints being unnecessary. Thus all geometrical parameters have been completely optimized at each stage of the

(3) Newton, M. D.; Ehrenson, S. *J. Am. Chem. Soc.* **1971**, *93*, 4971.
(4) Scheiner, S. *J. Am. Chem. Soc.* **1981**, *103*, 315.
(5) Scheiner, S. *J. Chem. Phys.* **1982**, *77*, 4039.
(6) Scheiner, S. *J. Phys. Chem.* **1982**, *86*, 376.
(7) Hillenbrand, E. A.; Scheiner, S. *J. Am. Chem. Soc.* **1984**, *106*, 6266.
(8) Allavena, M.; Tapia, O.; Evleth, E. M. *J. Phys. Chem.* **1985**, *89*, 1581.
(9) Scheiner, S.; Redfern, P.; Szczesniak, M. M. *J. Phys. Chem.* **1985**, *89*, 262.
(10) Szczesniak, M. M.; Scheiner, S. *J. Phys. Chem.* **1985**, *89*, 1835.
(11) Scheiner, S.; Hillenbrand, E. A. *J. Phys. Chem.* **1985**, *89*, 3053.
(12) Scheiner, S. *Acc. Chem. Res.* **1985**, *18*, 174.
(13) Hillenbrand, E. A.; Scheiner, S. *J. Am. Chem. Soc.* **1986**, *108*, 7178.
(14) Scheiner, S.; Redfern, P. *J. Phys. Chem.* **1986**, *90*, 2969.
(15) Carbonell, E.; Andrés, J. L.; Lledós, A.; Durán, M.; Bertrán, J. *J. Am. Chem. Soc.* **1988**, *110*, 996.
(16) Cybulski, S. M.; Scheiner, S. *J. Am. Chem. Soc.* **1989**, *111*, 23.
(17) Izatt, R. M.; Hansen, L. D.; Rytting, J. H.; Christensen, J. J. *J. Am. Chem. Soc.* **1965**, *87*, 2760.
(18) Birnbaum, G. I.; Giziewicz, J.; Huber, C. P.; Shugar, D. *J. Am. Chem. Soc.* **1976**, *98*, 4640.
(19) Watson, J. D.; Hopkins, N. H.; Roberts, J. W.; Steitz, J. A.; Weiner, A. M. *Molecular Biology of the Gene*; The Benjamin/Cummings Pub. Co.: Menlo Park, CA, 1987; pp 1106-1109.
(20) DePuy, C. H.; Bierbaum, V. M.; Schmitt, R. J.; Shapiro, R. H. *J. Am. Chem. Soc.* **1978**, *100*, 2920.
(21) Bierbaum, V. M.; Schmitt, R. J.; DePuy, C. H.; Mead, R. D.; Schulz, P. A.; Lineberger, W. C. *J. Am. Chem. Soc.* **1981**, *103*, 6262.
(22) Lledós, A.; Bertrán, J. *Tetrahedron Lett.* **1981**, *22*, 775.
(23) Lledós, A.; Bertrán, J. *J. Mol. Struct. Theochem.* **1985**, *120*, 73.
(24) Bertrán, J.; Lledós, A.; Revetllat, J. *Int. J. Quantum Chem.* **1983**, *23*, 587.
(25) Yamabe, T.; Yamashita, K.; Kaminoyama, M.; Koizumi, M.; Tachibana, A.; Fukui, K. *J. Phys. Chem.* **1984**, *88*, 1459.
(26) Bertrán, J.; Lledós, A. *J. Mol. Struct. Theochem.* **1985**, *123*, 211.
(27) Lledós, A.; Bertrán, J.; Ventura, O. N. *Int. J. Quantum Chem.* **1986**, *30*, 587.
(28) Ventura, O. N.; Lledós, A.; Bonaccorsi, R.; Bertrán, J.; Tomasi, J. *Theor. Chim. Acta* **1987**, *72*, 175.
(29) Ruelle, P.; Kesselring, V. W.; Nam-Tran, H. *J. Mol. Struct. Theochem.* **1985**, *124*, 41.
(30) Ruelle, P.; Kesselring, V. W.; Nam-Tran, H. *J. Am. Chem. Soc.* **1986**, *108*, 371.
(31) Ruelle, P. *Chem. Phys.* **1986**, *110*, 263.
(32) Ruelle, P. *J. Comput. Chem.* **1987**, *8*, 158.
(33) Ruelle, P. *J. Am. Chem. Soc.* **1987**, *109*, 1722.
(34) Nguyen, M. T.; Ruelle, P. *Chem. Phys. Lett.* **1987**, *138*, 486.
(35) Williams, I. H.; Spangler, D.; Femec, D. A.; Maggiora, G. M.; Schowen, R. L. *J. Am. Chem. Soc.* **1983**, *105*, 31.
(36) Williams, I. H. *J. Am. Chem. Soc.* **1987**, *109*, 6299.
(37) Nguyen, M. T.; Hegarty, A. I. *J. Am. Chem. Soc.* **1984**, *106*, 1552.
(38) Andrés, J. L.; Durán, M.; Lledós, A.; Bertrán, J. *Chem. Phys. Lett.* **1986**, *124*, 177.
(39) Frisch, M. J.; Binkely, J. S.; Schlegel, H. B.; Raghavachari, K.; Melius, C. F.; Martin, R. L.; Stewart, J. J. P.; Bobrowicz, F. W.; Rohlfing, C. M.; Kahn, L. R.; DeFrees, D. J.; Seeger, R.; Whiteside, R. A.; Fox, D. J.; Fleuder, E. M.; Pople, J. A. *Gaussian 86*; Carnegie-Mellon Quantum Chemistry Publishing Unit, Pittsburgh, PA, 1984.
(40) Spitznagel, G. W.; Clark, T.; Chandrasekhar, J.; Schleyer, P. von R. *J. Comput. Chem.* **1982**, *3*, 363.
(41) Clark, T.; Chandrasekhar, J.; Spitznagel, G. W.; Schleyer, P. von R. *J. Comput. Chem.* **1983**, *4*, 294.

Table II. 3-21+G IRC for the Intramolecular Proton Transfer in the Hydroperoxide Anion[a]

point	S^b	energy[c]	R(O–O′)[d]	R(O–H)[d]	R(O′–H)[d]	Q_O[e]	$Q_{O'}$[e]	Q_H[e]
R	−2.1	0.0	1.56	0.97	1.99	−0.70	−0.67	+0.37
37	−1.9	0.7	1.60	0.97	1.97	−0.73	−0.64	+0.37
35	−1.8	1.3	1.62	0.97	1.95	−0.73	−0.64	+0.37
33	−1.7	2.1	1.62	0.97	1.94	−0.73	−0.64	+0.37
31	−1.6	3.2	1.64	0.97	1.89	−0.74	−0.64	+0.38
25	−1.3	7.5	1.67	0.97	1.77	−0.75	−0.64	+0.39
23	−1.2	9.4	1.67	0.97	1.73	−0.76	−0.64	+0.40
19	−1.0	13.6	1.69	0.97	1.64	−0.77	−0.64	+0.41
17	−0.9	15.9	1.69	0.97	1.59	−0.77	−0.65	+0.42
15	−0.8	18.3	1.69	0.98	1.54	−0.78	−0.65	+0.43
13	−0.7	20.8	1.70	0.99	1.48	−0.79	−0.65	+0.44
11	−0.6	23.2	1.70	1.00	1.43	−0.79	−0.66	+0.45
9	−0.5	25.6	1.70	1.01	1.38	−0.79	−0.66	+0.45
7	−0.4	27.8	1.70	1.03	1.33	−0.78	−0.67	+0.45
5	−0.3	29.8	1.70	1.05	1.28	−0.78	−0.68	+0.46
TS	0.0	32.6	1.70	1.15	1.15	−0.73	−0.73	+0.46

[a] O and O′ stand for the proton donor and acceptor oxygen atoms, respectively. [b] In amu$^{1/2}$ bohr. [c] Relative energy with respect to reactant in kcal/mol. [d] In angstroms. [e] In au.

proton transfer. Geometry optimization and direct location of stationary points have been done with the Schlegel gradient optimization algorithm.[42] Analytical second derivatives of the energy with respect to the Cartesian coordinates[43] were computed to test the nature of each stationary point: no negative eigenvalue for an equilibrium structure and one negative eigenvalue for a transition state.

In order to test the effect of expanding the basis sets, the energies of the stationary points for both reactions of the hydroperoxide anion were recalculated with 6-31+G and 6-31+G (D, P) basis sets, the 3-21+G geometries being kept unchanged. Moreover the influence of correlation energy was determined by using the Møller–Plesset perturbation theory to second (MP2) and third orders (MP).[44]

Very useful information on the reaction mechanism can be obtained following the evolution of the geometrical and electronic parameters of the system along the reaction path. To perform this we have constructed the intrinsic reaction coordinate (IRC)[45-47] for the hydroperoxide anion reactions. The IRC has been computed with the GAMESS program[48] going downhill from the transition state in mass-weighted Cartesian coordinates.[49,50] The unique mode with imaginary frequency determines the starting direction away from the transition state. Assuming the harmonic approximation, we choose the initial step size Δs that produces the appropriate energy lowering $k(\Delta s)^2/2$, where k is the negative force constant associated with the imaginary frequency. Then the IRC is followed taking successive very small steps in the direction of the negative gradient, which is equivalent to the Euler method.

III. Intramolecular Proton Transfer in HO_2^-

The geometries of the stationary points localized on the 3-21+G potential energy hypersurface are shown in Figure 1. The R structure is a minimum and corresponds to the reactant. It is an asymmetric molecule, one O–H bond distance being noticeably lesser than the other. The geometry obtained here agrees well with a previous ab initio MCSCF calculation,[51] the O–O bond distance being slightly overestimated. The TS structure is a first-order saddle point corresponding to the transition state. It presents a C_{2v} symmetry, both O–H bond distances having become equal. In this case we have also depicted the transition vector, that is, the eigenvector associated with the negative eigenvalue. One can observe that it entirely corresponds to the proton transfer, both oxygen atoms being fixed. Finally, since the reaction is symmetric the product is the mirror image of the reactant and has not been represented.

Table I presents the potential energy barriers found at different levels of calculation. The first row shows the potential energy barrier obtained at the 3-21+G level, the stationary points having been localized on the 3-21+G potential energy hypersurface. The values of the potential energy barriers recalculated with larger basis sets and then including electron correlation, the 3-21+G geometries being kept unchanged, are exhibited in the second to seventh rows.

The most significant global point in Table I is that the potential energy barrier is very high at all levels of calculation, in such a way that the intramolecular proton transfer in the hydroperoxide anion appears to be very difficult under thermal conditions. In addition, comparison between rows reveals interesting methodological aspects. Regarding the effect of expanding the basis set, the situation is somewhat different than the one found by Scheiner[52-54] for other proton transfers, in which enlargements of the basis set invariably lead to higher energy barriers. In the present case, the 6-31+G barrier is higher than the 3-21+G one, but the energy barrier decreases when polarization functions on all atoms are incorporated. On the other hand, electron correlation provokes a notable diminution of the energy barrier, in good agreement with the Scheiner results.[16,52-54] As is well-known, the MP2 level tends to exaggerate the effect of electron correlation, in this way leading to underestimated energy barriers here.

To get a deeper insight on the mechanism of this reaction we have constructed the 3-21+G IRC starting from the transition state. The distance measured along the IRC is denoted by s, whose units are amu$^{1/2}$ bohr. The transition state is located at $s = 0$, and negative or positive values of s indicate the reactant or product region of the reaction, respectively. Due to the symmetry of the system only half of the IRC corresponding to the reactant side has had to be computed. An initial step size $\Delta s = 0.09$ amu$^{1/2}$ bohr that produces a harmonic energy lowering of 0.0005 hartree has been chosen. Then the step size $\Delta s = 0.05$ amu$^{1/2}$ bohr has been used. The relative energies with respect to the reactant, bond distances, and Mulliken charge on the three atoms at several points along the IRC are given in Table II. Proton-donor and proton-acceptor oxygen atoms are respectively denoted by O and O′.

From the geometrical point of view the reaction from the reactant ($s = -2.1$) to the transition state ($s = 0.$) proceeds clearly in two phases. In the first phase the O–O′ bond distance is lengthened while the O–H bond distance remains practically unchanged. The decrease of the O′–H bond distance arises from

(42) Schlegel, H. B. *J. Comput. Chem.* **1982**, *3*, 214.
(43) Pople, J. A.; Krishnan, R. A.; Schlegel, H. B.; Binkely, J. S. *Int. J. Quantum Chem., Quantum Chem. Symp.* **1979**, *13*, 225.
(44) Pople, J. A.; Binkley, J. S.; Seeger, R. *Int. J. Quantum Chem., Quantum Chem. Symp.* **1976**, *10S*, 1.
(45) Truhlar, D. G.; Kupperman, A. *J. Am. Chem. Soc.* **1971**, *93*, 1840.
(46) Fukui, K. *J. Phys. Chem.* **1970**, *74*, 4161.
(47) Fukui, K. *Pure Appl. Chem.* **1982**, *54*, 1825.
(48) Dupuis, M.; Spangler, D.; Wendoloski, J. J. *National Resource for Computations in Chemistry Software Catalogue*, Program QG01, 1980.
(49) Schmidt, M. W.; Gordon, M. S.; Dupuis, M. *J. Am. Chem. Soc.* **1985**, *107*, 2585.
(50) Garrett, B. C.; Redmon, M. J.; Steckler, R.; Truhlar, D. G.; Baldridge, K. K.; Bartal, D.; Schmidt, M. W.; Gordon, M. S. *J. Phys. Chem.* **1988**, *92*, 1476.
(51) Cohen, D.; Basch, H.; Osman, R. *J. Chem. Phys.* **1984**, *80*, 5684.
(52) Szczesniak, M. M.; Scheiner, S. *J. Chem. Phys.* **1982**, *77*, 4586.
(53) Scheiner, S.; Szczesniak, M. M.; Bigham, L. D. *Int. J. Quantum Chem.* **1983**, *23*, 739.
(54) Cybulski, S. M.; Scheiner, S. *J. Am. Chem. Soc.* **1987**, *109*, 4199.

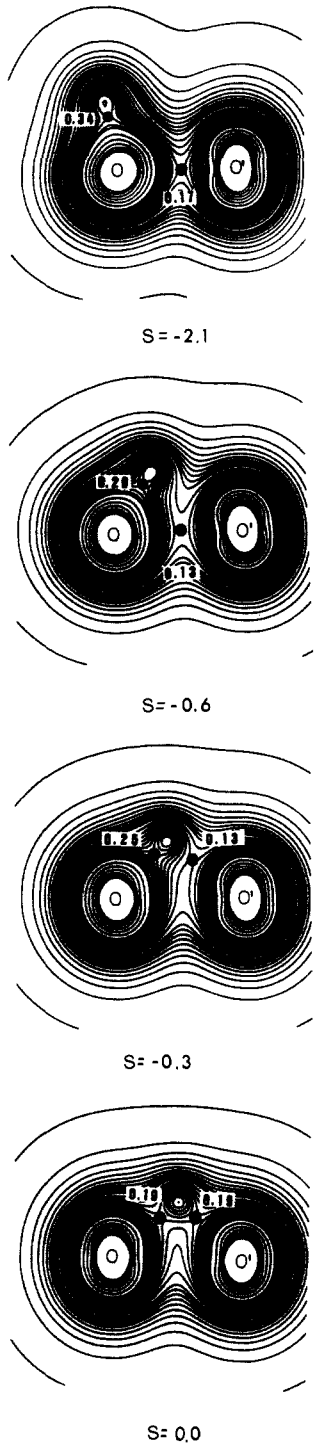

Figure 2. Isodensity contour plots of $\rho(\vec{r})$ in the plane of the hydroperoxide anion at selected structures along the IRC. Numbers indicate the $\rho(\vec{r})$ values at the bond critical points. O and O′ stand for the proton-donor and proton-acceptor oxygen atoms, respectively.

the diminution of the HOO′ angle. This phase concludes at about $s = -0.7$, where O–O′ bond distance is 1.70 Å, requiring about 21 kcal/mol, which involves most of the energy barrier. In a second phase both oxygen atoms are frozen while the O–H and O′–H bond distances are respectively lengthened and shortened, in such a way that both become equal at the transition state. Thus this second phase consists only of the motion of the proton in accordance with the transition vector mentioned above.

More revealing details can be obtained by analyzing the evolution of the electronic distribution along the reaction path. To this aim in Table II we have included the net charge associated with each atom along the IRC, arising from a Mulliken population analysis. Furthermore, an analysis of the topology of the total

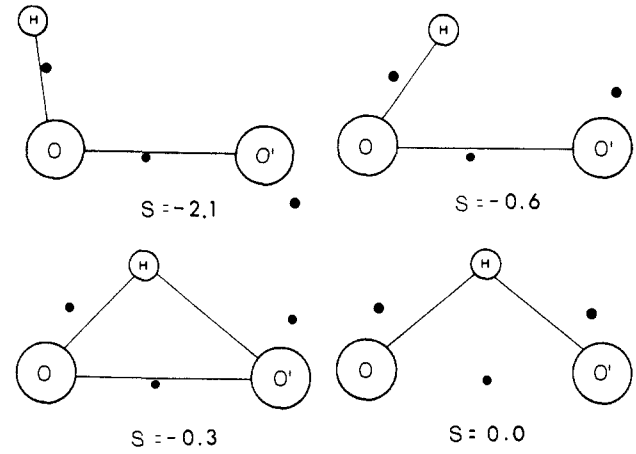

Figure 3. Evolution of the three centroids of charge directly related to the bonds at selected points along the IRC for the intramolecular proton transfer in HO_2^-. O and O′ stand for the proton-donor and proton-acceptor oxygen atoms, respectively.

electronic charge density $\rho(\vec{r})$, according to Bader's methodology,[55] has been done. Figure 2 presents the isodensity contour plots of $\rho(\vec{r})$ in the plane of hydroperoxide anion at selected structures along the IRC. The positions of the bond critical points have been marked by a dot. A bond critical point is a minimum along a single pair of gradient paths that are originated at the critical point and terminates one at each of the nuclei of the neighboring atoms but a maximum with respect to any orthogonal displacement. The existence of such a point indicates that the neighboring atoms are bonded to one another.

Simultaneous inspection of the last three columns of Table II and of Figure 2 provides valuable information. At the reactant ($s = -2.1$) the negative net charge of the molecule lies in both oxygen atoms, the hydrogen atom remaining positive. Only the O–O′ and O–H covalent bonds exist. No covalent bond appears between the proton-acceptor oxygen atom and the hydrogen atom. Since these two atoms possess net charges of opposite sign we can assume that a hydrogen bond is formed between them. The change of the electronic charge density at the bond critical points indicates that both O–O′ and O–H covalent bonds are weakened as the reaction proceeds. Until $s = -0.5$ the O–H bond is becoming more polarized, both the negative charge of the O atom and the positive charge of H atom increasing in absolute value, while the charge of the O′ atom keeps practically constant. At $s = -0.3$ two units separated by a very flat zone can be distinguished in the molecule: the O–H group and the O′ atom. The system could be visualized like a O–H dipole, electrostatically interacting with the negative charge localized in the O′ atom. If there is a bond critical point between both units it seems to be already connecting the H atom with the proton-acceptor oxygen atom O′. This is just the moment where O–O′ bond disappears and the O′–H covalent bond appears. At the transition state ($s = 0$) the O–O′ bond is completely broken, while the hydrogen atom is covalently and symmetrically bonded with both oxygen atoms, its positive charge reaching here the maximum value along the IRC.

From the previous analysis several interesting features of this reaction merit emphasis. For linear proton transfers like O–H···O′ it is generally admitted[7] that the energy barrier increases as the two oxygen atoms are further separated from one another. However, the hydroperoxide anion is a very different system because both oxygen atoms are initially bonded and the hydrogen bond H–O′ is not linear. In this case the motion of the proton provokes an important rearrangement of the electron density in such a way that the O–O′ bond is broken and both atoms are spontaneously separated. The high-energy barrier is probably caused by this breakage. On the other hand, in spite of the overall negative charge of the hydroperoxide anion, the hydrogen atom

(55) Bader, R. F. W.; Tal, Y.; Anderson, S. G.; Nguyen-Dang, T. T. *Isr. J. Chem.* **1980**, *19*, 8.

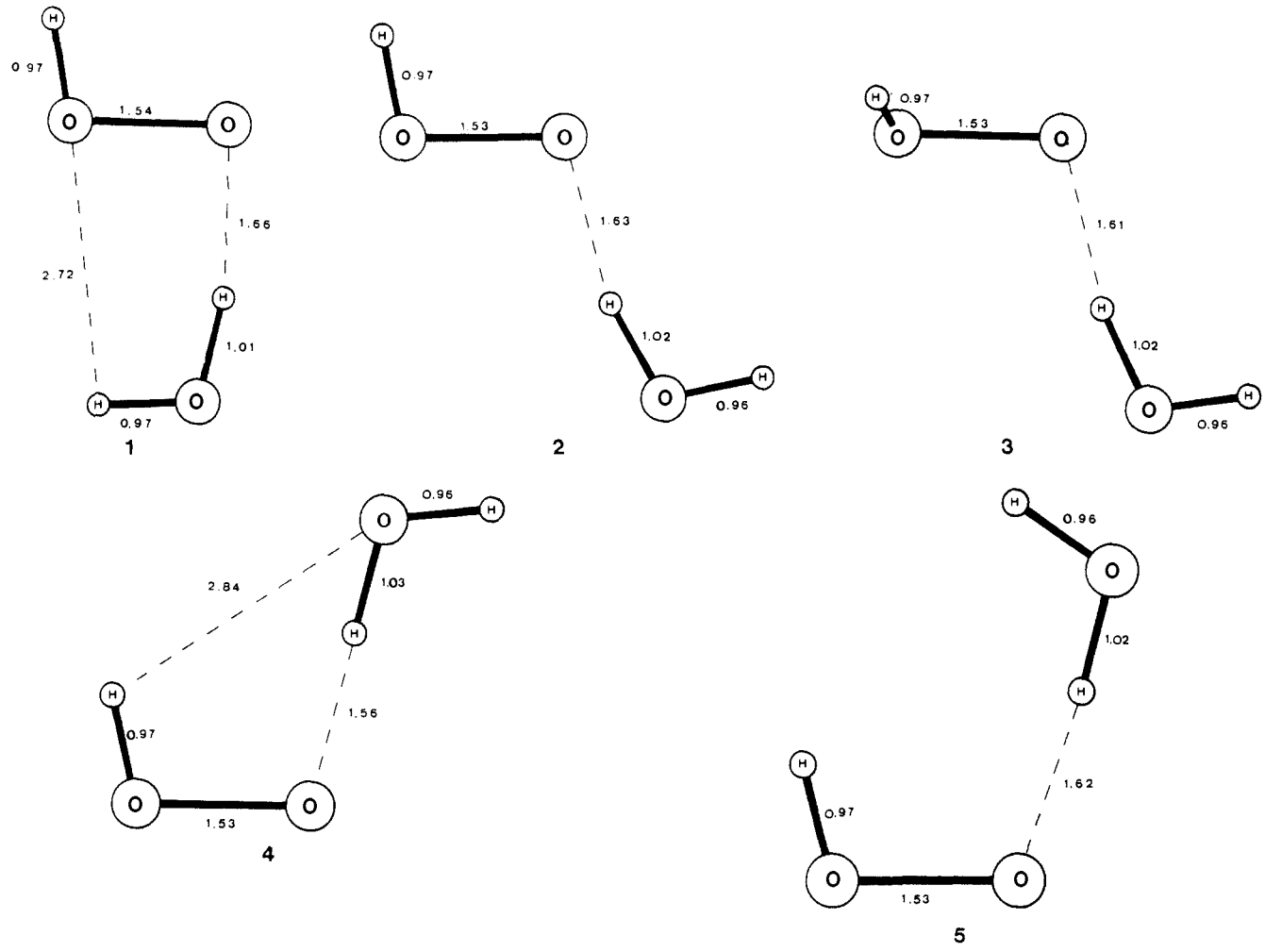

Figure 4. Geometries of the five stationary points that could be potentially stable conformers of the water–hydroperoxide anion complex.

always remains positive, its charge taking the maximum value at the transition state. This seems to indicate that it is really a proton.

To verify this last statement we have used the localization method of Foster–Boys.[56] This method allows localized molecular orbitals to be obtained and the positions of the centroids of negative charge associated with them to be calculated. Given that the hydroperoxide anion is a closed-shell molecule with 18 electrons, 9 centroids are obtained. Six of them are moving only slightly along the IRC: two centroids correspond to the oxygen inner shells and the other four are oxygen lone pairs. In Figure 3 we have only depicted the three centroids directly related to the bonds at selected points along the IRC. One can observe that the displacement of centroids occurs in the direction opposite to the motion of the proton, thus confirming the nature of the transferring particle. The evolution toward the proton of one of the centroids to form the new O′–H bond is particularly interesting. It has to be noted that a similar electron density migration has been previously reported.[5-7,57]

IV. Intramolecular Proton Transfer in the Water–Hydroperoxide Anion Complex

The situation is much more complicated when a water molecule is included in the model. In order to determine the structure of the water–anion complex we have explored the 3-21+G potential energy hypersurface. In Figure 4 five stationary points that could be potentially stable conformers are shown. They can transform each other by suitable rotations. In all cases but structure **3**, the water molecule lies on the hydroperoxide plane. Structures **1** and **2** correspond to the conformers previously found by Gao et al.[58] using the 6-31G (D) basis set. However, the diagonalization of the hessian matrix demonstrates that only structure **1** is a true 3-21+G minimum. Structures **2** and **3** are saddle points of first order, that is, their hessians possess one negative eigenvalue. Structures **4** and **5** are saddle points of second order, with two negative eigenvalues. All eigenvectors related to negative eigenvalues correspond to out-of-plane motions of the hydrogen atoms.

Let us now turn our attention to the proton transfer reaction. According the above results structure **1** in Figure 4 will be considered as the reactant. The reaction can be represented in the scheme below

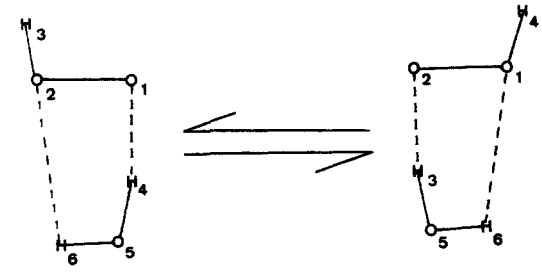

where we have introduced the numeration that we will use from here on in this section. This is also a symmetric reaction along which a double proton exchange of hydrogen atoms 3 and 4 occurs. When this process was studied an unexpected result was found. The reaction proceeds in two steps through two planar transition states with one planar intermediate between them. The corre-

(56) Foster, J. M.; Boys, S. F. *Rev. Mod. Phys.* **1960**, *32*, 296, 300.
(57) Sakai, S.; Morokuma, K. *J. Phys. Chem.* **1987**, *91*, 3661.
(58) Gao, J.; Garner, D. S.; Jorgensen, W. L. *J. Am. Chem. Soc.* **1986**, *108*, 4784.

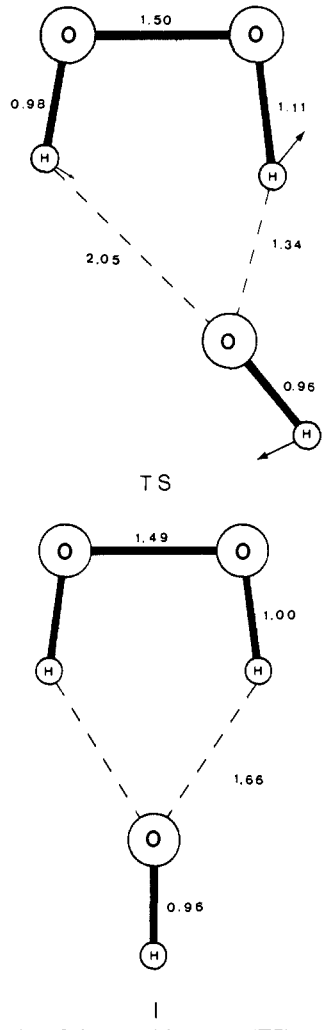

Figure 5. Geometries of the transition state (TS) and intermediate (I) for the water–hydroperoxide anion system. Arrows in the TS structure indicate the main components of the transition vector.

sponding structures are shown in Figure 5. Since both transition states are mirror images of one another only the first transition state has been presented. The first step consists of the transfer of hydrogen 4 from the water oxygen to the hydroperoxide ion. The transition vector reflects this motion and leads to the formation of water again in one direction and to the formation of intermediate in the opposite one. At the intermediate, with C_{2v} symmetry, the water oxygen is ready to approach 3 in order to remove it through the second transition state, where it will form water and lead to the final product. The existence of this intermediate is probably due to the fact that it is just a hydroxide ion solvated by a cis hydrogen peroxide slightly distorted. It should be mentioned that the cis conformer of hydrogen peroxide in the gas phase is not a 3-21+G minimum. However, when the intermediate is formed the simultaneous existence of two hydrogen bonds stabilizes the complex. It is worthy to note that in each step the transferring hydrogen atom maintains a positive net charge of about 0.55 au.

From the energetic point of view Table III presents the potential energy values for the first transition state and the intermediate, obtained at different levels of calculation. We recall that the values for the first and second transition states are identical. As noted above, calculations have been done with use of the 3-21+G localized structures. The most striking result is that the energy barrier has been drastically lowered due to the intervention of the water molecule, in such a way that now the proton transfer is low enough to be able to occur thermally. With regard to the effect of extending the basis set and introducing electron correlation, the same trends noted in the gas phase also appear here.

One of the most curious features of the present system emerges when the first transition state (or equivalently the second one)

Table III. Potential Energy[a] Barriers for the Intramolecular Proton Transfer in the Hydroperoxide Anion–Water System

	TS	intermediate
$\Delta E^{\ddagger}$(3-21+G//3-21+G)	7.6	7.1
$\Delta E^{\ddagger}$(6-31+G//3-21+G)	9.4	7.9
$\Delta E^{\ddagger}$(6-31+G(D,P)//3-21+G)	5.5	4.4
$\Delta E^{\ddagger}$(MP2/6-31+G//3-21+G)	3.6	2.0
$\Delta E^{\ddagger}$(MP2/6-31+G(D,P)//3-21+G)	-1.0	-1.7
$\Delta E^{\ddagger}$(MP3/6-31+G//3-21+G)	5.7	4.0
$\Delta E^{\ddagger}$(MP3/6-31+G(D,P)//3-21+G)	0.9	0.1

[a] In kcal/mol.

is allowed to be wholly optimized along both directions of the transition vector. In one direction the intermediate is obtained as expected. But the optimization does not take us to the reactant in the opposite direction. In effect, a planar saddle point of second order is attained. We want to stress that this is due to the fact that the C_s symmetry of the system is preserved in going in the direction of the gradient. However, hydrogen atoms 3 and 6 need to go out of the molecular plane in order to get the reactant. When the IRC is computed, a branching point arises, from which the reactant can be reached. This feature along with the existence of the stationary points presented in Figure 4 show the complexity of this 3-21+G potential energy hypersurface. More technical details of this IRC have been given elsewhere.[59]

To aid in understanding of this double proton exchange the isodensity contour plots of $\rho(\vec{r})$ in the molecular plane for the reactant, transition state, and intermediate are presented in Figure 6. Two structural units corresponding to water and hydroperoxide anion can be clearly distinguished at the reactant. Two hydrogen bonds exist between them, but only the O_1–H_4 one has a weak covalent interaction. At the transition state hydrogen 4 already has been transferred, although a covalent bond with oxygen 5 remains. It must be emphasized that this is just the moment when a very weak covalent bond between oxygen 5 and hydrogen 3 begins to appear, preparing in this way the second proton transfer. As a consequence, the formation of a ring point is initiated. At the intermediate again two structural units can be clearly defined, now corresponding to hydroxide anion and hydrogen peroxide. The existence of two hydrogen bonds with a covalent contribution stabilizes the system. The ring point appears completely formed in the middle of the system. This ring point is a minimum of $\rho(\vec{r})$ on the molecular plane but a maximum in the orthogonal direction and denotes the formation of a closed chain of bond paths linking the five nuclei around it.

Finally, it is interesting to note that the intervention of the water molecule prevents the breaking of the O–O bond in the hydroperoxide fragment along the reaction. Conversely to the gas-phase case studied in the previous section, this O–O bond is becoming somewhat shorter and stronger as the reaction proceeds from the reactant to the intermediate, in this way the energy barrier being noticeably less. In two consecutive steps the water molecule first transfers and then accepts a proton, acting then as a bifunctional catalyst. This demonstrates that the water molecule plays a very active role in this reaction, being an important part of the reaction coordinate.

V. Intramolecular Proton Transfer in the Glycolate Anion

Since this is also a symmetric process only the reactant side of the reaction will be explicitly treated. In Figure 7 the geometries of the stationary points localized on the 3-21+G potential energy hypersurface are shown. The reactant is not planar, the molecule being somewhat rotated about the C–C bond. A hydrogen bond exists between the proton (net charge = 0.49 au) and the proton-acceptor oxygen atom (net charge = −0.88 au). The transition state is a C_{2v} structure, both O–H bond distances being equal. The transition vector corresponds completely to the proton motion, the rest of the nuclei keeping fixed. The transferred hydrogen possesses a positive net charge of 0.49 au.

(59) Bosch, E.; Moreno, M.; Lluch, J. M.; Bertrán, J. *Chem. Phys. Lett.* **1989**, *160*, 543.

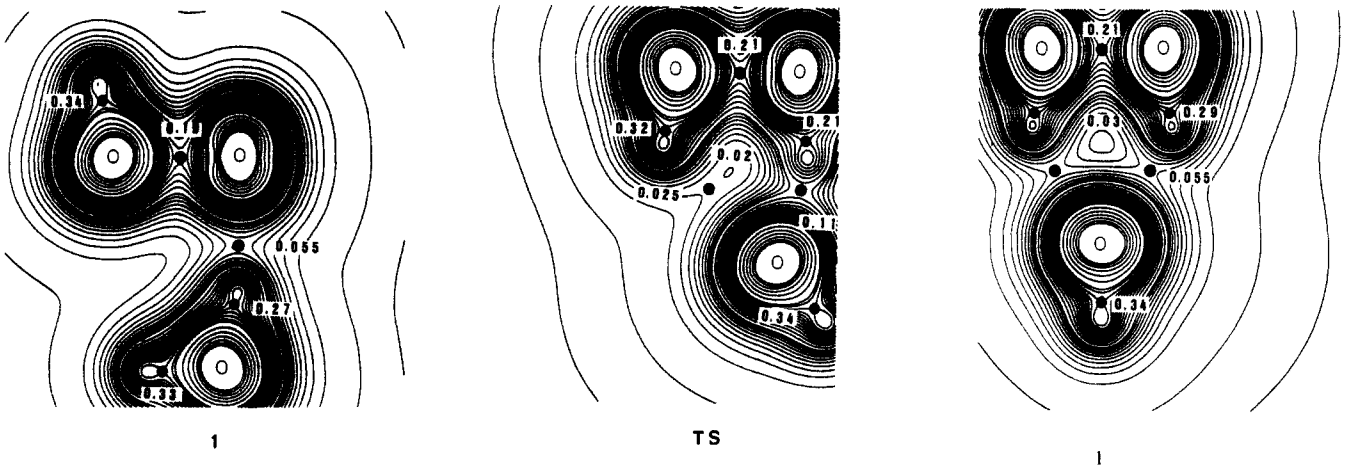

Figure 6. Isodensity contour plots of $\rho(\vec{r})$ in the molecular plane at the reactant (1), transition state (TS), and intermediate (I) for the water–hydroperoxide anion system. Numbers indicate the $\rho(\vec{r})$ values at the bond critical and ring points.

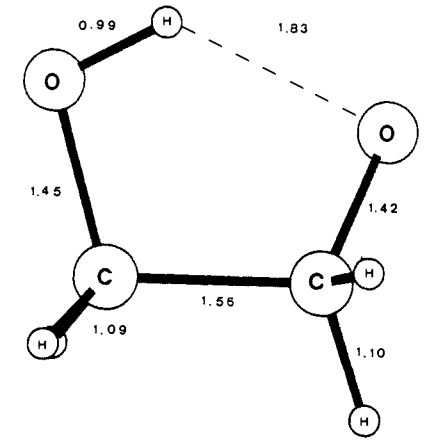

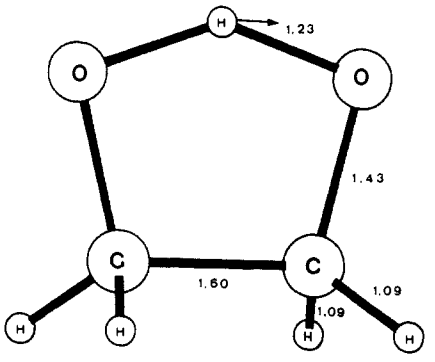

Figure 7. Geometries of the reactant (R) and transition state (TS) for the intramolecular proton transfer in the glycolate anion. The arrow in the TS structure indicates the transition vector.

To discuss the electronic distribution of the transition state, the isodensity contour plot of $\rho(\vec{r})$ in the heavy atoms plane has been depicted in Figure 8. One can observe that a ring point appears, which indicates again the existence of a closed chain of bond paths linking all five nuclei around it.

From the energetic point of view, the potential energy barrier is calculated to be 3.54 kcal mol^{-1} at the 3-21+G level, a value notoriously low.

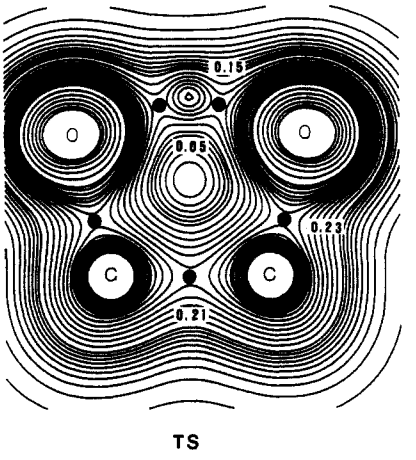

Figure 8. Isodensity contour plots of $\rho(\vec{r})$ in the heavy atoms plane at the transition state for the intramolecular proton transfer in the glycolate anion. Numbers indicate the $\rho(\vec{r})$ values at the bond critical and ring points.

VI. Conclusions

In this paper three intramolecular proton transfers between oxygen atoms in negatively charged systems have been studied. One of the most important features of this reaction is the rearrangement of the electronic charge density as the transfer proceeds. When the proton is approaching a region of space, an intense migration from this region toward the transferring proton is produced. This provokes a polarization of the bonds that lie in the vicinity of the proton trajectory. In the hydroperoxide anion reaction the proton moves close to the O–O bond, the corresponding polarization being strong enough to break this bond at the transition state. As a consequence, the energy barrier is very large. Conversely, a double proton exchange takes place when a water molecule participates on the reaction, the O–O bond not being broken. The water molecule acts as a bifunctional catalyst, significantly reducing the energy barrier. In the glycolate anion reaction, since both oxygen atoms are not linked to each other, the proton keeps far from the remaining bonds of the molecule, the electronic rearrangement leading to a ring point at the transition state, which indicates the existence of a closed chain of bond paths linking all five nuclei around the ring. In this way the energy barrier is very low.

Registry No. HO_2^-, 14691-59-9; $HO_2^-\cdot H_2O$, 103148-13-6; glycolate anion, 666-14-8.